Infacon XVI: International Ferro-Alloys Congress,
Edited by A.N. Wærnes, G. Tranell, M. Tangstad, E. Ringdalen, and C. van der Eijk
SINTEF/NTNU/FFF, Trondheim, 27-29 September 2021

Isothermal reduction of Nchwaning Manganese ore in $CO/CO_2/H_2$ atmospheres

T.L. Schanche[1], and M. Tangstad[1]
[1]NTNU, Norway, Trygve.l.schanche@ntnu.no
[2]NTNU, Norway, merete.tangstad@ntnu.no

Keywords: Manganese ore, prereduction, modeling, hydrogen

Abstract – In the industrial production of manganese ferroalloys, incomplete pre-reduction of higher manganese- and iron oxides in the furnace causes an excess consumption of carbon and energy. Pre-treatment of the manganese raw materials in an external unit may alleviate this issue. To optimize the pre-treatment process, a deeper understanding the solid-state reduction kinetics is needed.

In this work, Nchwaning manganese ore have been reduced isothermally at different temperatures at two different oxygen partial pressures in CO/CO_2 and $CO/CO_2/H_2$ gas mixtures, that is four different gas compositions. Isokinetic modeling was used to identify the activation energy range for the different cases and rate expressions were derived using the reaction order model. The derived model expressions adequately reproduced the experimental curves.

The effects of temperature and gas composition were quantified based on the model expressions. By reducing the CO content in the CO/CO_2 gas mixtures from 70 % to 30 %, the reduction rate was reduced by a factor 3. For the equivalent change in the $CO/CO_2/H_2$ gas mixtures, the rate was reduced by a factor 2. The addition of hydrogen increased the reaction rate by a factor of 1.9-2.8 for gases with equivalent thermodynamic potential within the experimental range. If partial combustion of the furnace gas is used to fuel a pretreatment unit, the addition of hydrogen will be beneficial to avoid significantly lowering the reduction rate of the ore.

INTRODUCTION

Manganese ferroalloys are mostly produced in submerged arc furnaces (SAF). Raw materials are charged from the top into the prereduction zone of the furnace. In the prereduction zone, the higher oxides of manganese and iron react with ascending CO gas from the coke-bed zone, reactions [1-6]. In addition to these reactions, decomposition of carbonates [7] will produce CO_2. Carbonates in the charge mixture often consists of Ca- Mg- and Mn-carbonates or dolomite. The Boudouard reaction (reaction [8]) will consume most of the CO_2 produced above about 800 °C consuming excess energy and carbon. (Olsen et al., 2007).

$$2MnO_2 + CO = Mn_2O_3 + CO_2 \qquad \Delta H°_{298K} = -201.8\,\frac{kJ}{mol} \qquad [1]$$

$$3Mn_2O_3 + CO = 2Mn_3O_4 + CO_2 \qquad \Delta H°_{298K} = -176.7\,\frac{kJ}{mol} \qquad [2]$$

$$Mn_3O_4 + CO = 3MnO + CO_2 \qquad \Delta H°_{298K} = -53.2\,\frac{kJ}{mol} \qquad [3]$$

$$3Fe_2O_3 + CO = 2Fe_3O_4 + CO_2 \qquad \Delta H°_{298K} = -39.6\,\frac{kJ}{mol} \qquad [4]$$

$$Fe_3O_4 + CO = 3FeO + CO_2 \qquad \Delta H°_{298K} = 37.4\,\frac{kJ}{mol} \qquad [5]$$

$$FeO + CO = Fe + CO_2 \qquad \Delta H°_{298K} = -17.9\,\frac{kJ}{mol} \qquad [6]$$

$$CaCO_3 = CaO + CO_2 \qquad \Delta H°_{298K} = 178,2\,\frac{kJ}{mol} \qquad [7]$$

$$C + CO_2 = 2CO \qquad \Delta H°_{298K} = 172,4\,\frac{kJ}{mol} \qquad [8]$$

$$MnO + C = Mn + CO \qquad \Delta H°_{298K} = 274.7\,\frac{kJ}{mol} \qquad [9]$$

Electronic copy available at: https://ssrn.com/abstract=3926158

The proportion of CO_2 from the reduction of Mn_3O_4 to MnO, Fe_3O_4 to metallic iron and decomposition of calcium carbonate reacting according to the Boudouard reaction defines the degree of pre-reduction (DPR) (Ishak and Tangstad, 2007). On an industrial scale, the typical DPR has been shown to be between 10 % and 40 % (Ishak and Tangstad, 2007). In figure 1, the excess energy and carbon consumption due to the Boudouard reaction has been calculated based on an industrial charge mixture. If the degree of prereduction can be increased from 40 % to 100 %, the carbon and energy consumption can be reduced by 76 kg and 303 kWh respectively per ton alloy produced.

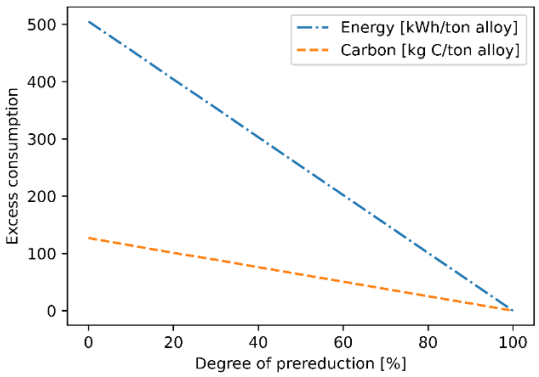

Figure 1: Calculated excess consumption of carbon and energy as a function of degree of prereduction. Calculated using the charge mixture in Tangstad et al., 2015.

One way to reduce the excess consumption of energy and carbon is to pretreat the raw materials in a pretreatment unit before they enter the furnace, as indicated in figure 2. The off gas from the SAF constitutes an excellent energy source for a pre-treatment unit due to its high CO content and its availability at the plant. However, the amount of gas produced under ideal conditions may not be sufficient to preheat and prereduce the ores sufficiently. If a MnO_2 ore is used, the amount of CO produced from reaction [9] will not be sufficient to remove the oxygen from the higher manganese oxides due to the fraction of MnO that remains in the slag. If full prereduction can be obtained in this case without adding additional reductant, the off-gas will consist of CO_2 and O_2. If a Mn_2O_3 ore is used, i.e. Nchwaning ore, the exothermal reactions may increase the temperature of the ore from room temperature to approximately 450 °C.

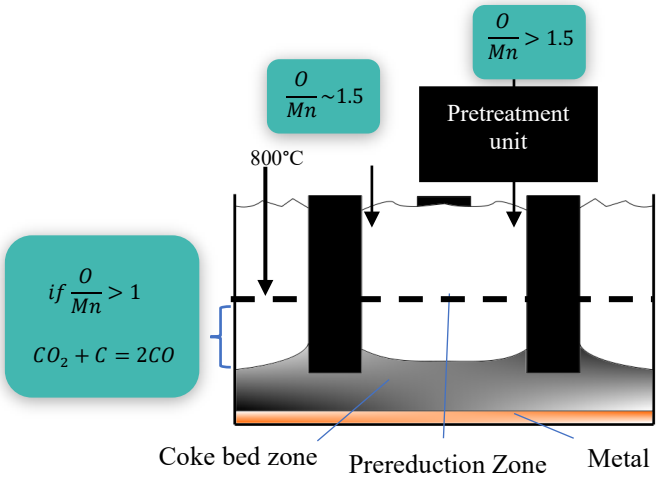

Figure 2: Shows a sketch of a submerged arc furnace where the input materials are added without and with pretreatment unit. Conceptually, the pretreatment unit should be placed near the furnace to avoid heat losses during material transfer.

Electronic copy available at: https://ssrn.com/abstract=3926158

Industrially, pre-reduction of manganese ore has been conducted in rotary kilns. Teguri et al., 2018, implemented pretreatment where the primary goal was to fully decompose all carbonates in the ore. HCMnFe furnace off-gas (70 % CO, 25 % CO_2, 5% H_2) and coke was used as fuel for the rotary kiln. Satisfactory removal of carbonates was achieved with a 9 h residence time in the reactor at 1150 °C - 1250 °C. In addition to the decomposition of carbonates, prereduction to O/Mn=1.19 (1 year average) was achieved. In another plant, a rotary kiln was used for heating and partial prereduction at lower temperatures 600 °C - 700 °C (Ishitobi et al., 2010). The rotary kiln was fueled by furnace off-gas, tire chips, coal and kerosene (Yoshida et al., 1998). Mass and energy balances has been calculated based on this unit (Tangstad et al., 2015). The effect of different states of prereduction on electrical energy consumption of the furnace can be seen in figure 3. Pretreatment reduces the electrical energy consumption and the magnitude of the reduction in consumption depends on the degree of which the exothermic reactions take place inside the furnace. Viewing the pretreatment unit and the furnace as one system, this effect cancels out since the exothermal reactions happening in the pretreatment unit will reduce the unit's energy consumption. The case of full external prereduction (rightmost column) has a relatively low power consumption due to the absence of the Boudouard reaction (reaction [8]).

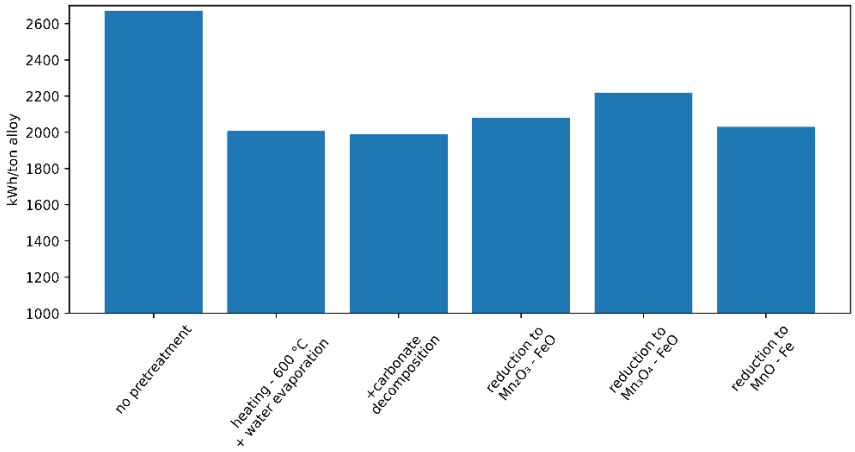

Figure 3: The electric energy consumption of a high carbon ferromanganese furnace based on mass and energy balances. The use of a pre-treatment unit with no, partial and complete pre-reduction of the raw materials is considered. Based on figure in (Tangstad et al., 2015)

Excessive moisture and excessive oxygen in the charge materials may lead to unstable furnace operation, i.e. furnace eruptions. There are safety limitations regarding the amount of moisture and excessive oxygen that enters the SAF (Pochart et al., 2007; Soller et al., 2010). By pre-treating the raw materials, the moisture will be removed, and higher oxides will be reduced, thus promoting stable furnace operation, and increasing the flexibility in the choice of charge mixture for production. Moisture in the raw materials have been seen to have a negative impact on the DPR (Ishak and Tangstad, 2007). In addition, pretreatment will increase the residence time of the raw materials at reducing conditions, improving the DPR (Swamy et al., 2001).

Several investigations have been done investigating the reactivity of manganese ores under simulated furnace conditions where the O/Mn ratio at 800 °C was used as the measure of reactivity (Ishak and Tangstad, 2007; Tangstad et al., 2010; Visser et al., 2013; Turkova et al., 2014; Jesus and Tangstad, 2020). In general, there is a positive correlation between porosity and reactivity, indicating that a lower mass transfer resistance within the materials improves the reduction rate. Ngoy et al., 2020 found that the addition of hydrogen to the reducing gas increased the reduction rate compared to CO/CO_2 mixtures at similar oxygen partial

Electronic copy available at: https://ssrn.com/abstract=3926158

pressures. Larssen, 2020, did non-isothermal reduction experiments on Nchwaning ore. The experiments were conducted with a fixed heating rate up to 1000 °C. Modeling of the experiments yielded the model expression shown in equation 10.

$$\frac{dX}{dt} = k_0 \exp\left(-\frac{E_a}{RT}\right)(1-X)p_{CO}^m r_p^n \quad [10]$$

Where k_0 [cm/atm·min]is the frequency factor , E_a [J/mol] is the activation energy, R [J/mol·K] is the universal gas constant, T [K] is temperature, p_{CO} [atm] is the CO partial pressure , r_p [cm] is the average particle size, n and m are constants, X is the degree of reduction and dX/dt is the reduction rate [1/min]. For Nchwaning ore, k_0=60.4 cm/atm·min, E_a =62.6 kJ/mol, m=1.5 and n=-1. The degree of reduction is based on the theoretical reduction of manganese and iron oxides to MnO and FeO in addition to the decomposition of carbonates. The decomposition of carbonates occurred in the temperature range 800-1000 °C. The dependency on particle size indicates that the reduction rate is affected by mass transfer.

In a pretreatment unit, furnace off-gas and other reductants may be used. A viable candidate for additional fuel is hydrogen. Hydrogen may be obtained from CO_2 neutral sources, thus reducing the carbon footprint of the production. In addition, hydrogen may improve the kinetics of reduction due to its diffusion properties. In this paper, the kinetics of Nchwaning ore has been investigated by isothermal reduction in CO/CO_2 and $CO/CO_2/H_2$ gas mixtures.

EQUILIBRIUM RELATIONS

Nchwaning is a high-grade oxide ore with a relatively low content of carbonates. The oxidation state of manganese in the ore is close to Mn_2O_3. The main manganese bearing minerals in Nchwaning ore are braunite I ($3(Mn,Fe)_2O_3 \cdot MnSiO_3$), and braunite II ($7(Mn,Fe)_2O_3 \cdot CaSiO_3$). It also contains minor amounts of manganite (MnOH), bixbyite (Mn_2O_3) and hausmannite (Mn_3O_4) (Larssen et al., 2020; Visser et al., 2013). Iron is found in in the braunites and as hematite (Fe_2O_3), and the carbonates consists mostly of $CaCO_3$ with minor content of complex Ca-Mg rich carbonates (Kleyenstuber, 1984; Visser et al., 2013). The possible sources of weight loss in the dry Nchwaning ore during heating in reducing atmosphere are reduction of oxides, evaporation of bound water and decomposition of carbonates.

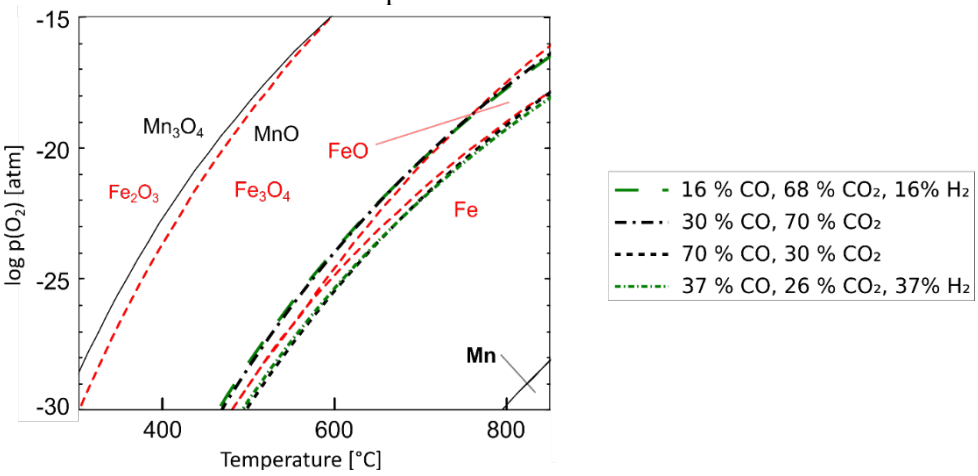

Figure 4: Phase diagram showing the Mn-O system (black solid lines) and the Fe-O system (red dashed lines) as a function of temperature and oxygen partial pressure. The equilibrium oxygen partial pressures used in the experiments have been superimposed on the phase diagram (see legend).

The phase diagram in figure 4 shows the equilibrium composition of the Mn- and Fe oxides as a function of temperature and oxygen partial pressure. It can be seen that Fe_3O_4 is stable for

Electronic copy available at: https://ssrn.com/abstract=3926158

the high pO_2 gas mixtures below ~ 750 °C whereas FeO is stable at higher temperatures. Metallic iron is stable for the low pO_2 gas mixtures and MnO is stable for all gas mixtures studied.

Figure 5 shows the phase stability in the Mn-Fe-O system as a function of composition and oxygen partial pressure at (a) 600 °C and (b) 800 °C. It can be seen that the oxides of manganese and iron display a wide range of solid solutions. The horizontal green band on the figures outlines the oxygen partial pressures of the used gas mixtures, and the vertical green line indicate the average composition of Nchwaning ores from the chemical analysis. Hence, the equilibrium composition of the manganese and iron oxides is MnO-FeO under the current experimental conditions.

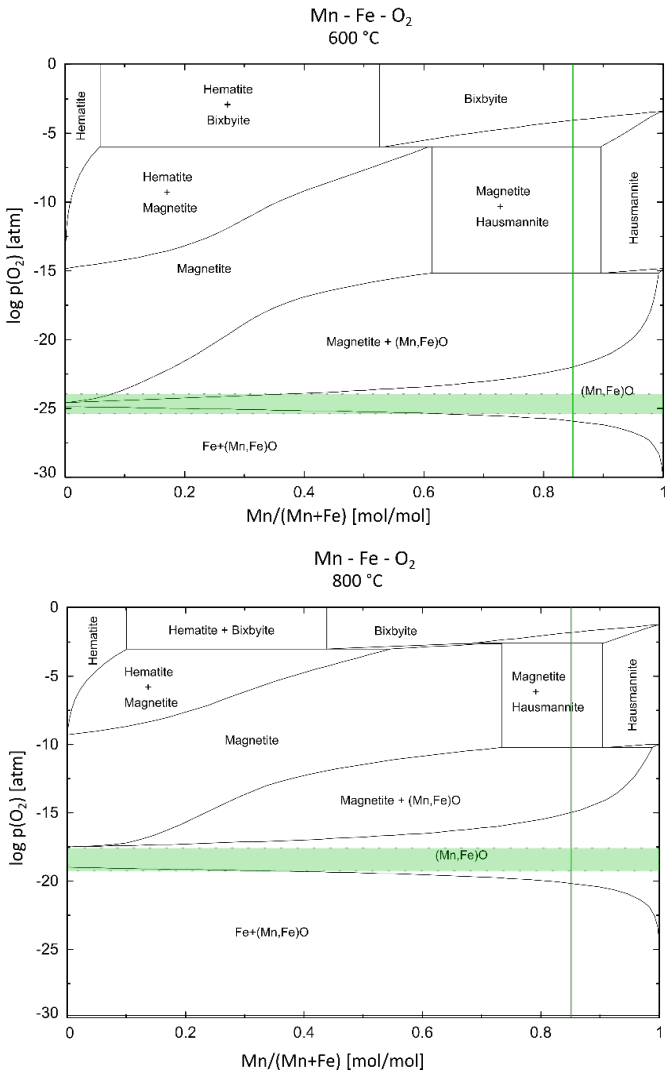

Figure 5: Phase diagram in the Mn-Fe-O system at 600 °C (a) and 800 °C (b) as a function of oxygen partial pressure and manganese-iron ratio. The highlighted area envelopes the oxygen partial pressures of the gas mixtures in this work, and the vertical line is the average composition based on chemical analysis.

Figure 6 shows the stability of some of the carbonates as a function of temperature and CO_2 partial pressure. The experimental conditions in this work is highlighted in figure 6. It can be seen that the carbonates of manganese and magnesium will readily decompose at the experimental temperatures and calcium carbonate will not. The phase diagrams in figures 4 ,5

Electronic copy available at: https://ssrn.com/abstract=3926158

and 6 have been calculated using Factsage 7.2 (Bale et al., 2016) and the oxygen partial pressures in figure 4 have been calculated using HSC Chemistry 9 (Roine, 2018).

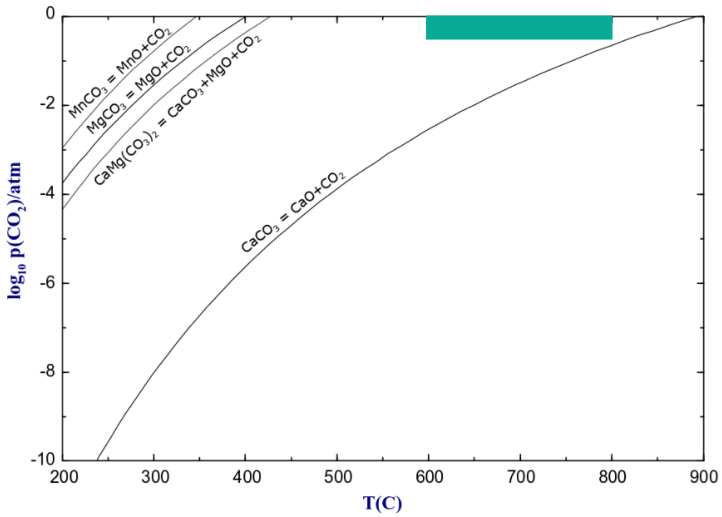

Figure 6: Shows the decomposition CO_2 partial pressure of $MnCO_3$, $MgCO_3$, $CaCO_3$ and $CaMg(CO_3)_2$ as a function of temperature.

EXPERIMENTAL PROCEDURE

Nchwaning manganese ore was crushed and sieved and the 9.52 – 15 mm fraction was selected for the experiments. The material was dried overnight at 105 °C to remove any surface moisture and representative samples of approximately 150 g were used for the experiments. The samples were analyzed by XRF and titriometry to determine the chemical composition and the oxygen associated with manganese respectively. CO_2 content was determined by combustion IR (ELTRA).

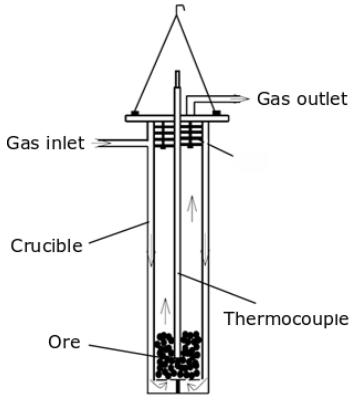

Figure 7: A sketch of the crucible used in the experiments.

A thermogravimetric furnace with a controllable atmosphere and off gas analyzer, was used for the experiments. A sketch of the crucible can be seen in figure 7. The furnace is heated to the desired temperature before it is raised to surround the crucible and the furnace temperature is kept constant throughout the experiment. The input gas is preheated in the double wall of the crucible before reaching the sample, figure 7. A thermocouple is placed in the center of the sample material to measure the sample temperature. The sample temperature, off-gas analysis and weight loss is continuously recorded. The samples were weighed on an external balance before and after the experiments. Due to drifting in the furnace balance, the weight loss was adjusted according to the external balance measurements. In addition,

Electronic copy available at: https://ssrn.com/abstract=3926158

oscillations in the balance following the movement of the furnace in the initial stages, were compensated for by zeroing the weight signal prior to observation of occurring reactions.

Experiments were run in two different CO/CO_2 mixtures containing 70 % CO and 30 % CO respectively. In addition, gas mixtures when H_2, CO and CO_2 were used where the volume of H_2 and CO was kept equal, and CO_2 was used to adjust oxygen partial pressure to get similar partial pressure as in the CO/CO_2 parallels. The total gas flow was 4 Nl/min for all experiments. The oxygen partial pressure of the gas mixtures was calculated from equation 11 and 12 using HSC Chemistry 9 (Roine, 2018), and can be seen in figure 4. Experiments were run for 210 minutes at 600 °C, 700 °C and 800 °C. The low pO_2 hydrogen containing gas at 600 °C experiment was not included in the results due to soot formation.

$$2CO(g) + O_2(g) = 2CO_2(g) \quad [11]$$

$$CO(g) + H_2O(g) = H_2(g) + CO_2(g) \quad [12]$$

RESULTS AND DISCUSSION

Figure 9a shows the temperature profile during three different experimental temperatures. There is an initial rapid increase of the temperature after the preheated furnace has been raised to surround the crucible. The sample reaches a peak temperature at the end of the heating period. The difference between the black dotted line (sample heated in argon) and the 800 °C curve shows the effect of the exothermal reactions on the sample temperature. The time to reach peak temperature as a function of the peak temperature for the experiments is shown in figure 9b. In addition to the heating from the furnace, the exothermic reactions develop energy, causing the temperature to reach a peak at 15-35 minutes after the furnace is raised.

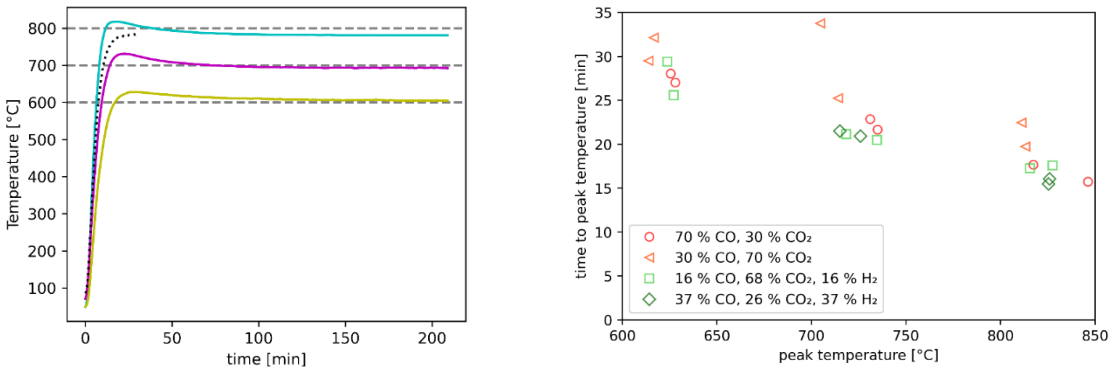

Figure 9: (a) Shows the measured sample temperature from the experiments reduced in 70 % CO – 30 % CO_2 atmosphere. Dashed lines at 600 °C, 700 °C and 800 °C have been added for comparison. The dotted black line is the temperature measured in a sample heated in argon. (b) Shows the peak temperature of the experiments and the time used to reach peak temperature.

Isothermal experiments are used to simulate a pre-treatment reactor that may run on a fixed temperature, hence isothermal experiments will be a closer simulation to this process. The conducted experiments were not truly isothermal due to the relatively long heating period (figure 9a and 9b) and due to the contribution from the exothermic reactions. The contribution from the exothermic reactions had the effect that the heating period for the highest temperatures was the shortest, even overshooting the desired temperature in the initial stages of the experiments.

Electronic copy available at: https://ssrn.com/abstract=3926158

Table I: Shows the mean and standard deviation from chemical analysis of three unreduced samples. The analysis was conducted by SINTEF Norlab.

	Unreduced sampls (n=3)		Reduced samples (n=37)	
	mean	**s**	**mean**	**s**
Mn	48,66	3,25	53,64	3,36
Fe	8,75	2,42	10,51	2,76
SiO_2	4,38	0,23	4,82	1,32
Al_2O_3	0,42	0,11	0,52	0,17
CaO	5,93	0,61	6,89	1,32
MgO	0,57	0,31	0,98	0,71
P	0,024	0,003	0,028	0,008
S	0,157	0,032	0,145	0,103
TiO_2	0,01	0,01	0,01	0,01
K_2O	0,00	0,00	0,03	0,04
BaO	0,57	0,17	0,57	0,42
MnO_2†	38,75	1,97	-	-
CO_2*	2,5	0,5	-	-

†Titrimetric *Combustion IR

To determine the chemical composition of the raw material, three samples of unreduced material (150 g) were selected for chemical analysis and the results can be seen in table I. The O/Mn ratio can be calculated from the reported MnO_2 and is found to be 1.50 ± 0.01. All excess oxygen above MnO is reported as MnO_2, however MnO_2 is not necessarily present, as in this case where O/Mn=1.5 corresponds to Mn_2O_3. The reduced samples were split in four, and one quarter was selected for chemical analysis. To compare the chemical analyses of the reduced samples, the oxygen above MnO-FeO and the CO_2 was removed in the calculations, after which the composition of the remaining constituents was adjusted accordingly. It can be seen from table I that the standard deviation is in the same order of magnitude as the unreduced ore despite that the increased number of samples, indicating that the ore is quite heterogeneous. Based on the analysis of the unreduced samples in table I, the theoretical weight loss of Nchwaning ore was calculated and is shown in table II, where the contribution from the different reaction steps also can be seen.

Table II: Contribution to the weight loss [wt %] from the manganese and iron oxides. Calculated based on the chemical analysis of the unreduced samples shown in table I.

Me = Mn, Fe	Mn	Fe	Sum
$Me_2O_3 \rightarrow Me_3O_4$	2.4 %	0.43 %	2.8 %
$Me_3O_4 \rightarrow MeO$	4.7 %	0.84 %	5.6 %
Sum	7.1 %	1.3 %	8.4 %

Figure 10a shows the measured weight loss as a function of the O/Mn ratio in the reduced samples. The theoretical weight loss from the reduction have also been added. From the figure it can be seen that, with the exception of the 30% CO – 70 % CO_2 parallel, the experiments conducted at 700 °C are clustered around the theoretical weight loss close to O/Mn=1 whereas the experiments conducted at 800 °C show a higher weight loss. Using the manganese content, iron content and O/Mn ratio from the chemical analysis of each sample, the expected weight loss due to reduction of oxides has been calculated. The calculation is done under the assumptions that iron and manganese is at the same state of oxidation and that the initial O/Mn ratio is 1.5, and can be seen in figure 10b, where it has been plotted against the measured weight loss.

Electronic copy available at: https://ssrn.com/abstract=3926158

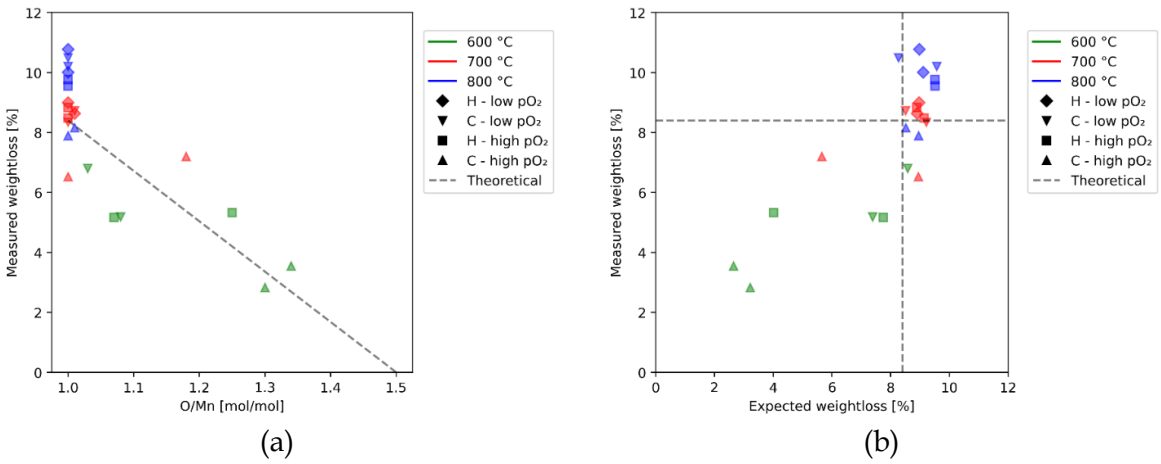

Figure 10: Shows the measured weight loss a function of (a) the O/Mn ratio of the reduced samples and (b) the expected weight loss based on the amount of manganese and iron in the chemical analysis of each sample.

Even though there still is some uncertainty in the data due to scattering and heterogeneity, it can be seen that the expected weight loss correlates with the measured weight loss, however the weight loss from the 800 °C experiments exceeded the expected weight loss for many of the experiments. This may be caused by several factors. Larssen, 2020 found that the weight loss due to evaporation of bound water was negligible and that carbonates decomposed above 800 °C. Even though that there is a relatively low content of CO_2 in the ore (table I), it contributes disproportionately to the total weight loss. Assuming all Mn initially is Mn_2O_3 and that all CO_2 is $CaCO_3$, the content of Mn_2O_3 and $CaCO_3$ is 69,9 g and 5.7 g respectively. If all the carbonates were to decompose, the weight loss would be slightly higher than the reduction of all Mn_2O_3 to Mn_3O_4 (2.5 % and 2.4 % respectively). It is possible that a fraction of the carbonates decomposed in the period where the sample temperature exceeded 800 °C, or that a significant fraction of the carbonates contains Mg cations, making it decompose at lower temperatures (figure 6). Another possible explanation to the difference of this weight loss is the state of the iron at the end of the experiment. Even though the phase diagram (figure 4) predicts metallic iron at low oxygen partial pressures, it is not expected to form, as seen in previous investigations (Fahim et al., 2013; Larssen, 2020; Lobo, 2015). It has also been observed that the reduction of Mn_3O_4 is about two orders of magnitude faster than the reduction of Fe_2O_3 at 900°C (Kor, 1978). From table II it is seen that the expected weight loss from the reduction of iron oxides to FeO is 1.3 %, where the reduction of Fe_3O_4 accounts for 0.84 %. These values correspond respectively to 15 % and 5 % of the total expected weight loss which is similar to the observed difference between the 700 °C and 800 °C experiments (figure 11).

Figure 11 shows the degree of reduction and the reduction rate from the experiments in the four different gas mixtures. The degree of reduction, α, is defined in equation 13 where w_0 is the initial weight [g], w_r is selected as the highest weight loss [g] achieved in the experiments and w(t) [g] is the measured weight as a function of time. The reduction rate is obtained by differentiating α with respect to time.

$$\alpha = \frac{w_0 - w(t)}{w_0 - w_r} \qquad [13]$$

As seen in figures 9a and b, the desired temperature was achieved 15-30 minutes into the experiment and the samples were reduced to some extent during the heating period (figure 11). For the CO/CO_2 experiments, (Figure 11 (a) and (c)), it can be seen that lowering the

Electronic copy available at: https://ssrn.com/abstract=3926158

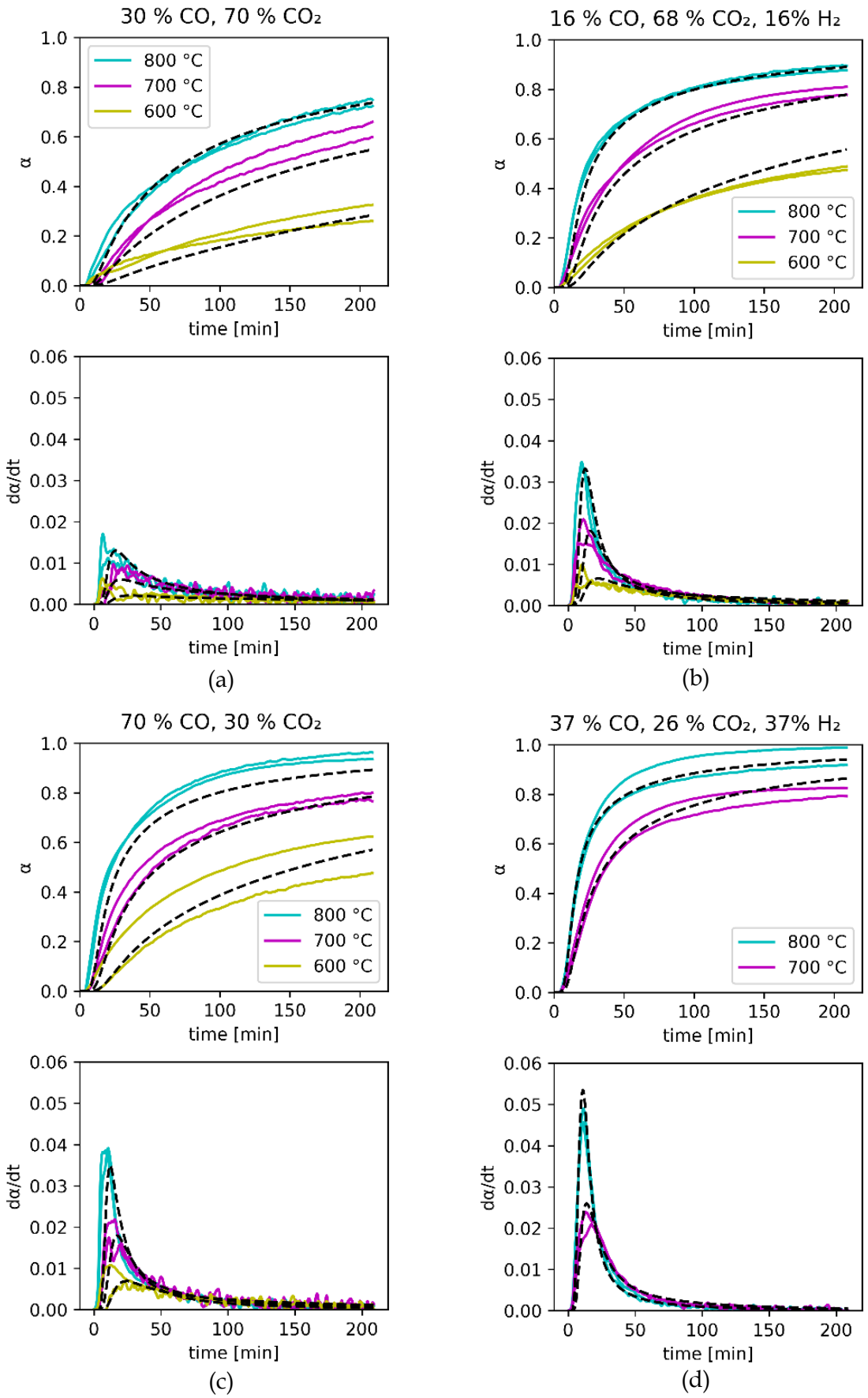

Figure 11: Conversion curve and reaction rate for the four gas mixtures. The dashed lines are predicted by the model equations 16 and 17.

Electronic copy available at: https://ssrn.com/abstract=3926158

oxygen partial pressure increases the reduction rate, approximately doubling the maximum value. The same tendency can be seen in the hydrogen containing parallels, (b) and (d), where maximum reduction rate is approximately 50 % higher for the low pO_2 experiments at 800 °C. For the high oxygen partial pressure experiments, figure 11 (a) and (b), the presence of hydrogen increases the reduction rate, approximately doubling the maximum reduction rate. For the low pO_2, (c) and (d), it can also be seen that the hydrogen increases the reduction rate at 800 °C, however at 700 °C, the difference is not that pronounced.

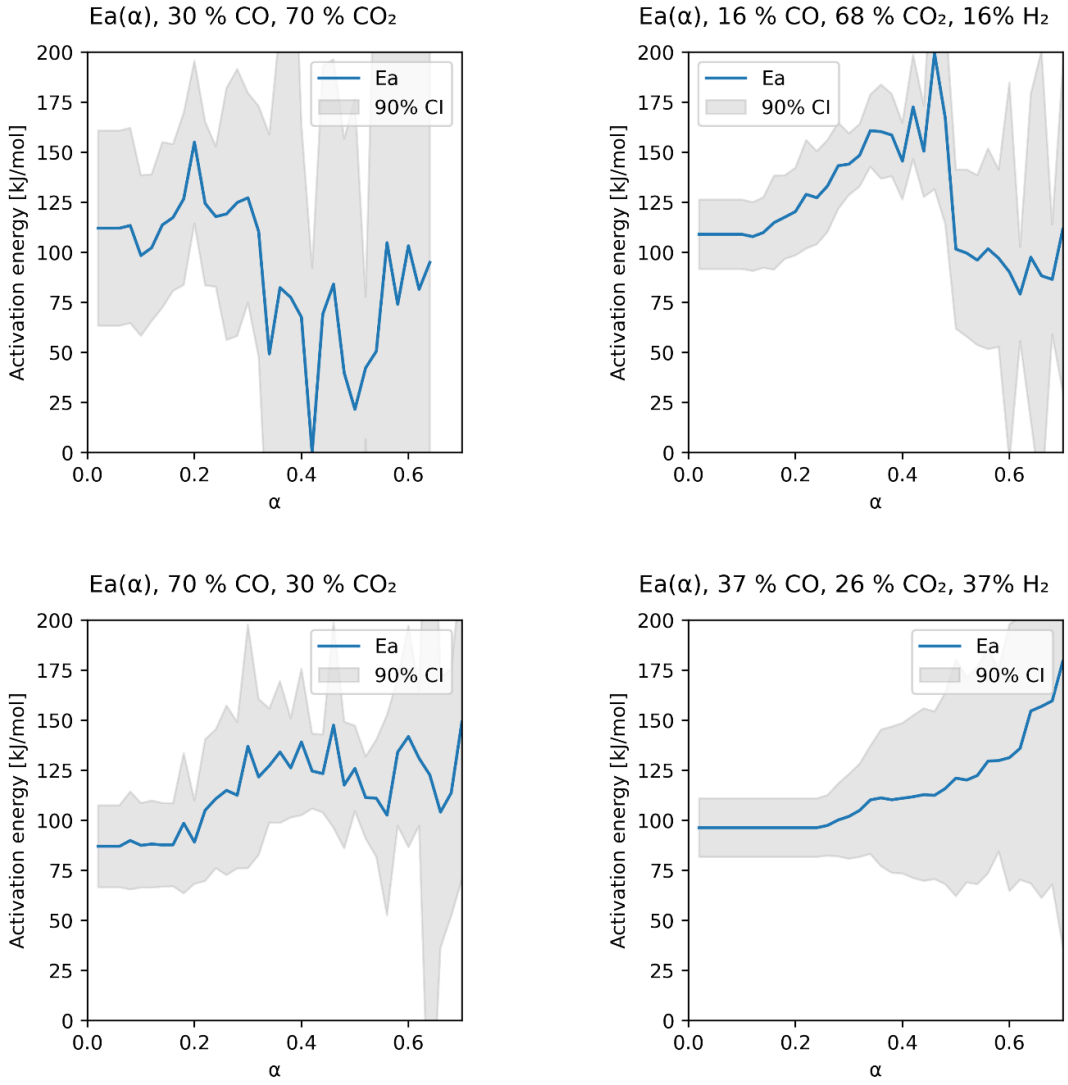

Figure 12: Shows the apparent activation energy as a function of degree of reduction for reduction in the different gas mixtures.

During reduction of the ore, reactions [2-6] happen simultaneously in parallel and/or in series. To detect changes in the contribution from different reaction steps, isoconversional modeling was utilized. According to the isoconversional principle, the reaction rate at a specific conversion is only a function of temperature (Vyazovkin et al., 2011). The apparent activation energy was calculated for fixed values of conversion within each gas mixtures with a stepsize of 0.02.

In figure 12, the calculated apparent activation energy is shown as a function of degree of reduction for the reduction in the different gas mixtures. After α=0.32 for the 30 % CO – 70 %

Electronic copy available at: https://ssrn.com/abstract=3926158

CO_2 parallel, results from only two temperatures contribute to the activation energy. This coincides with a significant drop in the activation energy and with the increased size of the confidence interval that can be seen in the figure. The same applies to the 16 % CO – 68 % CO_2 – 16 % H_2 parallel after about α=0.48 and the 70 % CO – 30 % CO_2 parallel after α=0.62. The 37 % CO – 26 % CO_2 – 37 % H_2 parallel calculations is based on two temperatures throughout the range. The isoconversional modeling indicates an increase in the apparent activation energy following the initial stages of reduction after which it was maintained or increased for the low oxygen partial pressure parallels. In the high oxygen partial pressure parallels, the apparent activation energy dropped to a lower level after the initial increase. Either case is an indication of a complex kinetic regime where two or more steps with different activation energies occur and the relative influence between them changes (Vyazovkin et al., 2011). The drop in activation energy for the high oxygen partial pressure parallels at high conversions may indicate that diffusion resistance increases its influence (Szekely et al., 1976) i.e. the mechanism shifts towards diffusion control, which is reasonable considering that the active species in those parallels are more dilute. Another explanation is that it may simply be a result of experimental noise, heterogeneity of the raw materials and few measurement points.

The real measured temperature was used for all modeling in this work, negating potential errors from temperature deviations. This type of experiment is designed to look at the overall kinetics of the pre-reduction process, so the purpose of modeling is to obtain a quantitative description of the prereduction process in different gas mixtures that includes the total contributions from all the prereduction reactions. To obtain this, a model was developed determining the kinetic parameters by fitting a model equation to the experimental data. The equation used for further modeling is shown in equation 14 where dα/dt [1/min] is the reduction rate, k_0 [1/min] is the apparent pre-exponential constant, E_a [J/mol] is the apparent activation energy, R [J/mol·K] is the universal gas constant, α is the degree of reduction and x is the reaction order. The modeling was done by a non-linear least squares method, fitting the model to the reduction rates using the measured temperatures from the experiments.

$$\frac{d\alpha}{dt} = k_0 \exp\left(-\frac{E_a}{RT}\right)(1-\alpha)^x \qquad [14]$$

The values of the pre-exponential factor, activation energy and reaction order that obtained the best fit for the various gas mixtures are given in table III. The obtained activation energies from the different gas mixtures averages 80 kJ/mol. The average reaction order is calculated to 1.9, and hence is 2 used in the later calculations. An activation energy of 80 kJ/mol is in a similar range as predicted by the isoconversional modeling. The deviation of the fitted values between the different gas mixtures may be explained by experimental noise and heterogeneity of the raw material.

Table III: The best fit values of pre-exponential constant, activation energy and reaction order for the different gas mixtures.

Gas mixture	CO-CO_2		CO-CO_2-H_2		
pO_2	low	high	low	high	Average
k_0 [1/min]	260	29	771	1044	n.d.
E_a [kJ/mol]	79	68	82	89	80
x	1.7	1.9	1.9	2.0	1.9

Based on the obtained fitting values, the fitting procedure was repeated with fixed values of reaction order and activation energy. Table IV shows the apparent pre-exponential constant for the different gas mixtures under the assumptions that the activation energy is 80 kJ/mol and that the reaction order is 2.

Electronic copy available at: https://ssrn.com/abstract=3926158

Table IV: Pre-exponential constant for the different gas mixtures under the assumptions E_a=80 kJ/mol and x=2.

gas	CO-CO2		CO-CO2-H2	
pO_2	low	high	low	high
k_0 [1/min]	360	119	677	339

Since the pre-exponential constants in table IV is modeled using the same reaction order and activation energy, their ratios directly reflect the effects on the rate. Reducing the oxygen partial pressure of the hydrogen free gas (increasing the CO content from 30 % to 70 %) triples the reduction rate at constant temperature, whereas for the hydrogen containing gas mixtures, the rate is doubled by reducing the oxygen partial pressure. The effect of hydrogen is an increase of the reduction rate of 2.8 times and 1.9 times at high and low oxygen partial pressure respectively.

To isolate the effect of the CO content in the CO-CO_2 gas mixtures, k_0 in equation 15 is separated into the apparent pre-exponential constant for the reactions, k, and the CO-content contribution according to the following relation:

$$k_0 = k\left(p_{CO}^m - \left(\frac{p_{CO_2}}{K}\right)^2\right) \cong k p_{CO}^m \qquad [15]$$

Where p_{CO} and p_{CO2} are the partial pressures of CO and CO_2 respectively, K is the equilibrium constant and m is the order of which the partial pressure of CO in the CO-CO_2 gas mixtures affect the reaction rate. The simplification in the latter part of the equation is valid under the assumption that the forward reaction is much larger than the back reaction. For reaction 3 the error by this assumption is less than 0.03 % in the experimental range. The H_2 containing parallels have an equal oxygen partial pressure, thus the thermodynamic driving force is the same as in the CO-CO_2 parallels. To compare the two, the driving force is represented as (1-p_{CO2}). The values of m and k are obtained by taking the slope and intercept of the linear regression of the plot ln(k_0) vs ln(1-p_{CO2}), which can be seen in figure 13. The corresponding rate equations for the CO-CO_2 gas mixtures and the CO-CO_2-H_2 gas mixtures can be seen in equation 16 and 17 respectively.

$$\frac{d\alpha}{dt} = 574 \cdot (1 - p_{CO_2})^{1.31} \exp\left(-\frac{80\,000}{RT}\right)(1-\alpha)^2 \qquad [16]$$

$$\frac{d\alpha}{dt} = 868 \cdot (1 - p_{CO_2})^{0.82} \exp\left(-\frac{80\,000}{RT}\right)(1-\alpha)^2 \qquad [17]$$

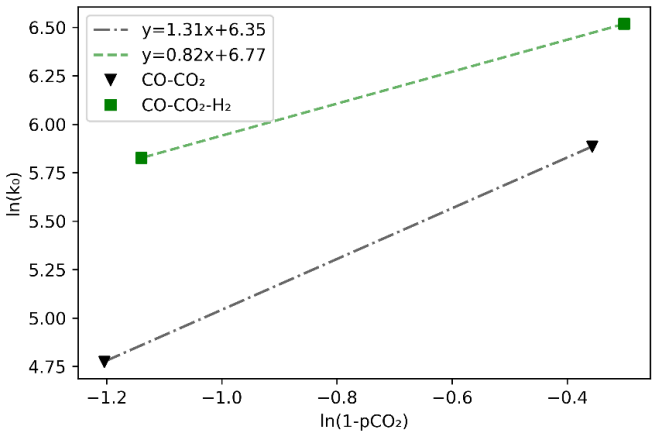

Figure 13: The natural logarithm of the pre-exponential constant vs the driving force for reduction, represented by (1-p_{CO2}).

Electronic copy available at: https://ssrn.com/abstract=3926158

To assess the validity of the models, the model equations have been plotted together with the conversion curves and the reaction rate in figure 11. It can be seen that the model predictions adequately represent the experimental data. A simple model is not sufficient to perfectly replicate the experiments, but it offers a simplistic approximation utilizing data from an experiment that also serves to simulate the pretreatment in a similar manner that it may be conducted industrially, albeit with a smaller particle size fraction of the material.

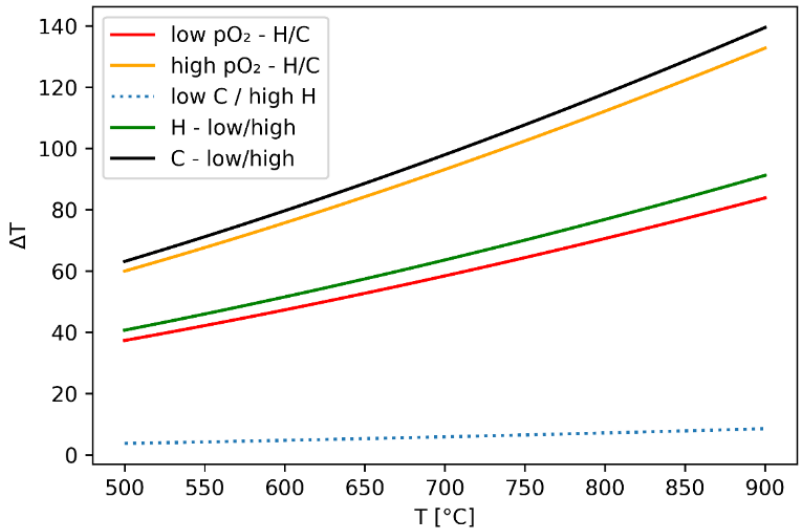

Figure 14: Shows the temperature increase needed to maintain the reduction rate if the partial pressure of oxygen is increased (low/high), hydrogen is added and a similar partial pressure is maintained (H/C) or oxygen partial pressure is increased together with the addition of hydrogen (low C / high H). H denotes hydrogen containing gas and C denotes hydrogen free gas.

The optimal utilization of furnace gas in a pretreatment unit is subject to many factors. As seen previously, the energy of the furnace gas alone may not be sufficient for increasing the temperature or for complete prereduction. With the addition of extra fuel, the temperature may be increased by partial combustion of the gas. However, this solution may not be optimal. If by partially combusting the furnace gas, the oxygen partial pressure is increased from the low to the high values used in this work the reduction rate will drop by a factor of 2-3. To obtain the same reduction rate as for the low oxygen partial pressure, the temperature needs to be increased by approximately 100 °C and 63 °C for the CO-CO_2 and CO-CO_2-H_2 mixtures in this work respectively. Figure 14 shows the necessary temperature increase to maintain the reduction rate for different combinations of gas mixtures. One interesting feature is that it is possible to increase the oxygen partial pressure of the furnace gas, i.e. by partial combustion, and compensating the loss in reduction rate almost completely by the addition of hydrogen, as seen in the blue dotted curve in figure 14.

The low oxygen partial pressure hydrogen containing gas showed the best reduction characteristics, however it may not be the best choice for a prereduction unit due to the soot produced at temperatures below 600 °C.

CONCLUSIONS

Nchwaning manganese ore was reduced isothermally in CO/CO_2 and $CO/CO_2/H_2$ gas mixtures and a model was derived to cover all prereduction reactions which adequately reproduced the experimental curves. From the model equations it was seen that increasing the

Electronic copy available at: https://ssrn.com/abstract=3926158

oxygen partial pressure of the reducing gas, significantly retarded the reduction rate of Nchwaning ore under the experimental conditions. The reduction rate was lowered by a factor of 2 and 3 for the $CO/CO_2/H_2$ and the CO/CO_2 gas mixtures respectively. Conversely, the addition of hydrogen significantly improved the reduction kinetics of Nchwaning ore, increasing the reaction rate by a factor of 1.9 and 2.8 for the low and high oxygen partial pressures respectively. The excellent properties of hydrogen make it feasible to conduct prereduction at lower temperatures compared to current industrial practice, in addition to reducing the carbon footprint of the process.

ACKNOWLEDGEMENTS

The authors gratefully acknowledge the financial support from Research Council of Norway (Project Code: 280968) and our industrial partners Elkem ASA, TiZir Titanium & Iron AS, Eramet Norway AS, Finnfjord AS and Wacker Chemicals Norway AS for financing KPN Reduced CO2 emissions in metal production project.

REFERENCES

Bale, C.W., Bélisle, E., Chartrand, P., Decterov, S.A., Eriksson, G., Gheribi, A.E., Hack, K., Jung, I.-H., Kang, Y.-B., Melançon, J., Pelton, A.D., Petersen, S., Robelin, C., Sangster, J., Spencer, P., Van Ende, M.-A., 2016. FactSage thermochemical software and databases, 2010–2016. Calphad 54, 35–53. https://doi.org/10.1016/j.calphad.2016.05.002

Fahim, M.S., El Faramawy, H., Ahmed, A.M., Ghali, S.N., Kandil, A.E.H.T., 2013. Characterization of Egyptian Manganese Ores for Production of High Carbon Ferromanganese. J. Miner. Mater. Charact. Eng. 01, 68–74. https://doi.org/10.4236/jmmce.2013.12013

Ishak, R., Tangstad, M., 2007. DEGREE OF PREREDUCTION WITHOUT COKE CONSUMPTION IN INDUSTRIAL FURNACES. Presented at the Infacon XI, New Delhi, India, p. 14.

Ishitobi, T., Ichihara, K., Homma, T., 2010. OPERATIONAL IMPROVEMENTS OF A SUBMERGED ARC FURNACE IN KASHIMA WORKS (KF-1) RELINED IN 2006, in: The Twelfth International Ferroalloy Congress. Presented at the Infacon XII, Helsinki, Finland, p. 8.

Jesus, L.G.M.D., Tangstad, M., 2020. CO Reactivity of Manganese Lumps Versus Briquettes. ISIJ Int. 60, 2129–2133. https://doi.org/10.2355/isijinternational.ISIJINT-2019-493

Kleyenstuber, A.S.E., 1984. The mineralogy of the manganese-bearing Hotazel formation, of the Proterozoic Transvaal Sequence in Griqualand West, South Africa. South Afr. J. Geol. 87, 257–272.

Kor, G.J.W., 1978. The thermal decomposition of Mn2O3 and the reduction of Mn3O4 by C and CO. Metall. Trans. B 9, 307–311. https://doi.org/10.1007/BF02653697

Larssen, T.A., 2020. Prereduction of Comilog- and Nchwaning-ore (PhD Thesis). Norwegian university of science and technology, Trondheim, Norway.

Larssen, T.A., Senk, D., Tangstad, M., 2020. Reduction of Manganese Ores in CO-CO2 Atmospheres. Metall. Mater. Trans. B. https://doi.org/10.1007/s11663-020-02018-0

Lobo, S., 2015. Reduction of manganese ores using CO, H2, CO2 and H2 blends (Internal report). Norwegian University of Science and Technology, Trondheim, Norway.

Ngoy, D., Sukhomlinov, D., Tangstad, M., 2020. Pre-reduction Behaviour of Manganese Ores in H2 and CO Containing Gases. ISIJ Int. 60, 7.

Olsen, S.E., Tangstad, M., Lindstad, T., 2007. Production of Manganese Ferroalloys. tapir academic press, Trondheim.

Pochart, G., Joncourt, L., Touchard, N., Perdon, C., 2007. METALLURGICAL BENEFIT OF REACTIVE HIGH GRADE ORE IN MANGANESE ALLOYS MANUFACTURING. Presented at the Infacon XI, New Delhi, India, p. 14.

Roine, A., 2018. HSC Chemistry®. Outotec, Pori.

Soller, A., Amalric, A., Pochart, G., Nussbaum, G., 2010. MANGANESE ORE AND ALLOYS PILOTING TOOLS AT ERAMET RESEARCH. Presented at the Infacon XII, Helsinki, Finland, p. 10.

Swamy, K.N., Robertson, D.G.C., Calvert, P., Kozak, D., 2001. Factors affecting Carbon Consumption in the Production of High Carbon Ferromanganese. Presented at the Infacon IX, Quebec City, Canada, p. 9.

Szekely, J., Evans, J.W., Sohn, H.Y., 1976. Gas-Solid Reactions. Academic press, New York, USA.

Tangstad, M., Ichihara, K., Ringdalen, E., 2015. PRETREATMENT UNIT IN FERROMANGANESE PRODUCTION. Presented at the Infacon XIV, Kyiv, Ukraine, p. 8.

Electronic copy available at: https://ssrn.com/abstract=3926158

Tangstad, M., Leroy, D., Ringdalen, E., 2010. BEHAVIOR OF AGGLOMERATES IN FERROMANGANESE PRODUCTION. Presented at the Infacon XII, Helsinki, Finland, p. 11.
Teguri, D., Saito, K., Miyauchi, Y., 2018. Manganese ore pre-reduction using a rotary kiln to manufacture super-low-phosphorus ferromanganese, in: Infacon XV: International Ferro-Alloys Congress. Presented at the Infacon XV, Cape Town, South Africa, p. 14.
Turkova, K., Slizovskiy, D., Tangstad, M., 2014. CO Reactivity and Porosity of Manganese Materials. ISIJ Int. 54, 1204–1208. https://doi.org/10.2355/isijinternational.54.1204
Visser, M., Smith, H., Ringdalen, E., Tangstad, M., 2013. PROPERTIES OF NCHWANINGAND GLORIA ORE IN THE PRODUCTION OF Mn FERRQ...ALLOYS. Presented at the Infacon XIII, Almaty, Kazakhstan, p. 14.
Vyazovkin, S., Burnham, A.K., Criado, J.M., Pérez-Maqueda, L.A., Popescu, C., Sbirrazzuoli, N., 2011. ICTAC Kinetics Committee recommendations for performing kinetic computations on thermal analysis data. Thermochim. Acta 520, 1–19. https://doi.org/10.1016/j.tca.2011.03.034
Yoshida, F., Honma, T., Sasaki, T., 1998. Automation and Reduction of Labor in the Operation of Electric Arc Furnace for HCFeMn Production, in: 8th International Ferroalloys Congress Proceedings. Presented at the Infacon VIII, Beijing, China, p. 6.

Trygve Lindahl Schanche
PhD Candidate, Norwegian University of Science and Technology (NTNU)
Trygve has a MSc in Materials Science and Engineering from NTNU (2013) and has previously worked in industry and as a chief engineer at NTNU. He started his PhD in 2018 and is working on the reduction of CO_2 emissions from manganese ferroalloy production by improving prereduction.

Electronic copy available at: https://ssrn.com/abstract=3926158